Growth and rapid succession of methanotrophs effectively limit methane release during lake overturn

Magdalena J. Mayr[1,2], Matthias Zimmermann[1,2], Jason Dey[1], Andreas Brand[1,2], Bernhard Wehrli[1,2], *Helmut Bürgmann[1]

[1]Eawag, Swiss Federal Institute of Aquatic Science and Technology, 6047 Kastanienbaum, Switzerland

[2]Institute of Biogeochemistry and Pollutant Dynamics, Department of Environmental Systems Science, ETH Zurich, 8092 Zurich, Switzerland

*Corresponding author: Helmut Bürgmann, Eawag, Seestrasse 79, 6047 Kastanienbaum, Switzerland, +41 58 765 2165, helmut.buergmann@eawag.ch

Abstract

Lakes and reservoirs contribute substantially to atmospheric concentrations of the potent greenhouse gas methane. Lacustrine sediments produce large amounts of methane, which accumulate in oxygen-depleted hypolimnia of stratified lakes. Due to climate change and progressing eutrophication, the number of lakes with hypolimnetic methane storage may increase in the future. However, whether stored methane eventually reaches the atmosphere during lake overturn is a matter of controversy and depends critically on the response of the methanotroph assemblage. We show that the methanotroph assemblage in a mixing lake underwent both a substantial bloom and ecological succession. As a result, the methane oxidation capacity of the mixed layer kept pace with the methane supplied from the hypolimnion and most of the stored methane was oxidized. This previously unknown aspect of freshwater methanotroph ecology represents an effective mechanism limiting methane transfer from lakes to the atmosphere.

Introduction

Lakes and impoundments emit a greenhouse gas (GHG) equivalent of 20% of the global fossil fuel CO_2 emissions, with methane contributing 75% of these CO_2 equivalents[1]. Stratified lakes accumulate the potent greenhouse gas methane in their oxygen-depleted bottom waters[2]. During lake overturn, stored methane may reach the surface layer, thereby running the risk of outgassing. Despite the established importance of lakes for global GHG emissions, the fate of methane during the overturn period is still a matter of controversy. Two competing hypotheses regarding the fate of accumulated methane have been proposed. According to the first line of thinking, most of the stored methane will be released into the atmosphere[3] as an emission pulse that adds to continuous methane fluxes across the water-air interface. According to the second hypothesis, methanotrophs oxidize most of the methane with oxygen to CO_2, a GHG which has a 34 times lower global warming potential for a 100-yr time-scale[4] and sequester a small proportion as biomass. Some previous estimates assumed overturn to occur on very short time scales, e.g. a single day[3] therefore favoring the first hypothesis. Other studies have indicated that lake overturn typically takes place on a scale of weeks to months, even in shallow lakes[5–7], which may allow time for significant methane oxidation. This controversy has not yet been fully resolved [8] and the role and ecological dynamics of methane-oxidizing bacteria (MOB) during lake overturn remains to be explored.

MOB in lakes have mostly been investigated during the stratified season, when a structured MOB assemblage forms an efficient methane converter preventing the methane accumulating in the bottom water from outgassing[9–12]. How the MOB assemblage responds to lake overturn remains unknown, but its growth rate and resulting methane oxidation capacity is critical for the amount of methane emitted. During lake overturn environmental conditions change compared to the stratified situation[13]. The lake cools down and oxygen and methane, which are vertically separated during stratification, become simultaneously available as water with different substrate concentrations mix in the expanding surface layer.

Here we present a field study covering the entire three months of the autumn lake overturn of shallow eutrophic Lake Rotsee, Switzerland. We asked (i) if the MOB assemblage grows fast enough to oxidize the methane mobilized from the bottom water before outgassing and (ii) whether the standing MOB assemblage is activated, or a new assemblage successively takes over in the changing lake. We used 16S rRNA gene amplicon sequencing, *pmoA* mRNA sequencing and qPCR, CARD-FISH and potential methane oxidation rate measurements to investigate succession, growth and methane oxidation capacity of the MOB assemblage during lake overturn. The rates of physical mixing and the transfer and transformation of methane have been analyzed with a process-based model in a parallel study[14].

The present study provides detailed insights into the dynamics of freshwater lake MOB during the critical overturn period. We show that a new and highly abundant MOB assemblage, representing up to 28% of 16S rRNA gene sequences, thrived in the expanding mixed layer. In parallel with MOB abundance, the methane oxidation capacity of the lake increased substantially, thereby limiting methane emissions to a small percentage of the stored methane.

Results

Characteristics of stratification and overturn dynamics

To determine the response of the MOB assemblage and methane oxidation activity to lake overturn, we sampled the shallow eutrophic Lake Rotsee at eight time points covering stratification, overturn and inverse stratification. The starting point of our sampling campaign on Oct 4, 2017 represents a typical stratified situation, which in Rotsee starts to develop in May[15]. In the following, we refer to the large amounts of methane that have accumulated during summer in the hypolimnion as 'stored methane'.

Most of the oxygen and stored methane in the water column were vertically separated from each other prior to lake overturn (Fig. 1A). The lake water cooled down from October to January, resulting in a gradual expansion of the mixed layer until December (Fig. 1B). By Dec 12, a cooler mixed layer formed on top of warmer bottom water (Fig. 1B), which has a slightly higher salinity (Supplementary Fig. 1).

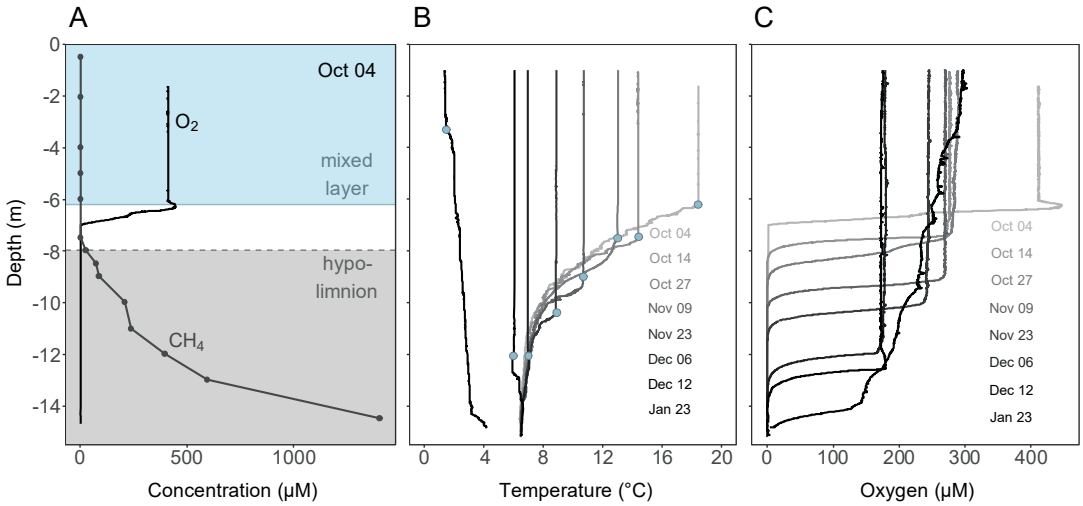

Figure 1 Stratification and progressive deepening of the mixed layer during lake overturn. Depth profiles of physicochemical parameters in Rotsee during the lake overturn period of 2017**. A)** Stratified situation in Rotsee prior to lake overturn. Oxygen in the mixed layer and methane in the hypolimnion are separated from each other. The methane-enriched hypolimnion (≥ 2 µM) is shaded in grey, the mixed layer is shaded in blue. **B)** Temperature profiles of the cooling lake in autumn and winter and the resulting expansion of the mixed layer at each sampling date. Blue dots indicate the mixed layer depth. In January an inverse stratification established. **C)** Corresponding oxygen profiles at each sampling date.

From October to December, a total of 4.2 Mg C (ref. 14) of stored methane gradually entered the expanding mixed layer (Supplementary Fig. 2). Nevertheless, median methane concentrations in the surface layer stayed low, ranging from 0.1 – 1.1 µM. During overturn, oxygen levels in the mixed layer dropped down to approx. 175 µM (Dec 12, Fig. 1C), likely due to methane and other reduced substances from the hypolimnion triggering abiotic and biotic oxygen consumption. From December to January, oxygen concentrations increased again.

The methane oxidizing assemblage prior to lake overturn

We analyzed the MOB assemblage with a set of independent and mutually supportive methods. We used 16S rRNA gene sequencing to phylogenetically identify known groups of MOB, to estimate their proportion among the bacterial community and to assess MOB assemblage dynamics. The *pmoA* mRNA sequencing combined with qPCR provided an independent assessment of the MOB assemblage as well as confirmation of transcriptional activity of the methane monooxygenase. To facilitate interpretation, we assigned the same colors to MOB ASVs (MOB-affiliated 16S rRNA amplicon sequence variants) and aaASVs (*pmoA* amino acid operational taxonomic units) in Fig 3 and 4 and supplementary figures, if they showed similar relative abundance and distribution pattern in a canonical correspondence analysis (Supplementary Fig. 3) and compatible placement within the phylogenetic trees (Supplementary Fig. 4).

On Oct 4, the proportion of MOB ASVs and the copy number of *pmoA* transcripts peaked at the upper boundary of the methane-enriched hypolimnion, although both measures showed that MOB were present throughout the water column (Fig. 2A, B). The hypolimnion harbored a higher proportion of MOB ASVs and more *pmoA* transcripts than the oxygen-rich mixed layer. Therefore, it represents a potential reservoir of MOB for the following lake overturn. The composition of the MOB assemblage differed strongly between the mixed layer and hypolimnion. The mixed layer was dominated by gammaproteobacterial type Ia MOB (Fig. 2A, B, blue) assigned to uncultivated groups CABC2E06/Lake cluster1 (ASV_5/aaASV1 and aaASV6). According to 16S rRNA gene-based analysis a *Methylocystis*

105 (ASV_354, yellow) was also dominant, however the corresponding aaASV7 *pmoA* transcript was rather

106 underrepresented (Supplementary Fig. 5).

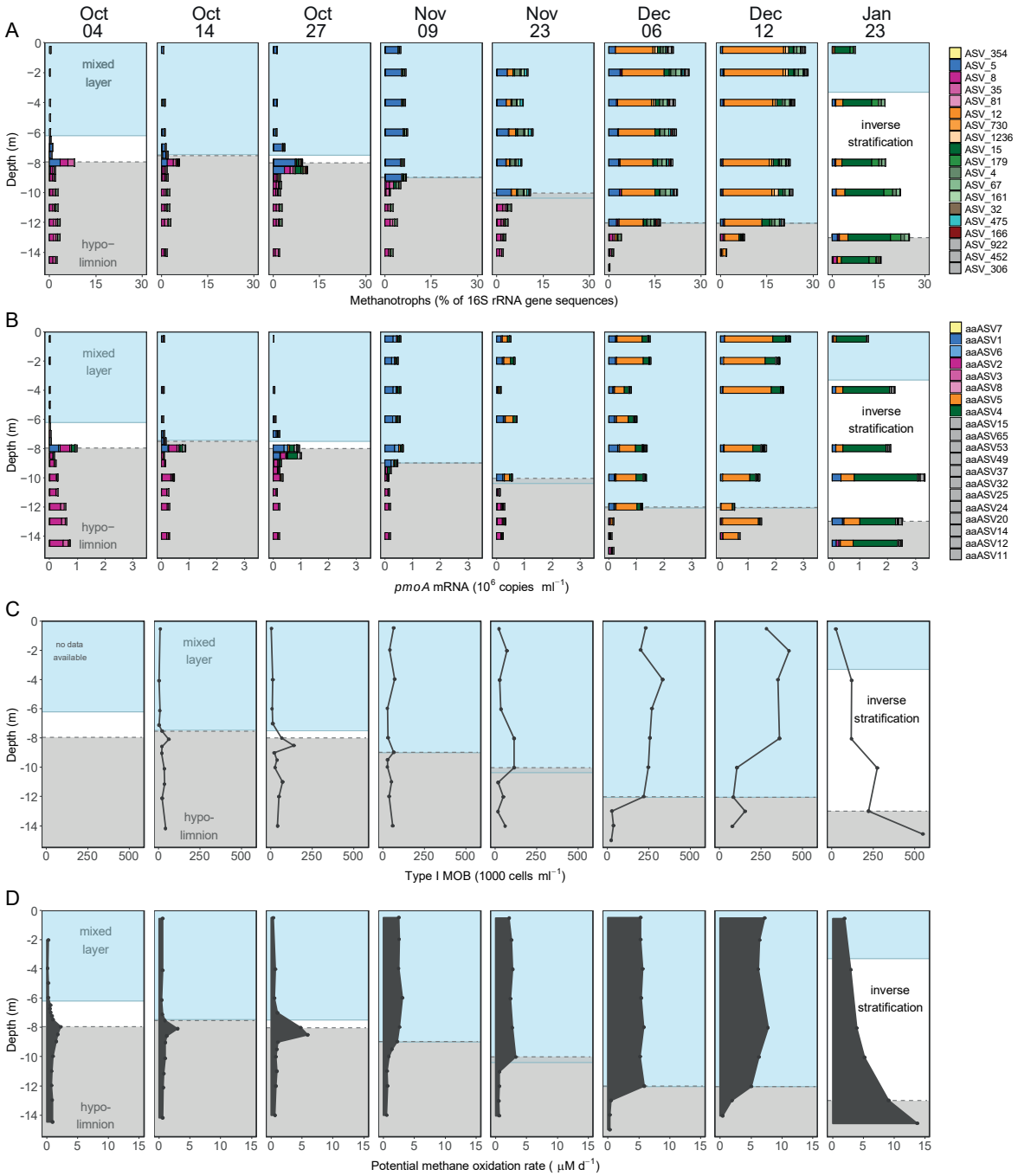

107

Figure 2 Depth distribution and dynamics of the MOB assemblage, *pmoA* transcripts, MOB cell numbers and potential methane oxidation rates during lake overturn. The mixed layer (blue background) depth increased with time, while the methane-rich hypolimnion starting at ≥ 2 µM CH_4, (gray background) got gradually incorporated into the mixed layer. **A)** Abundance and composition of MOB from 16S rRNA gene amplicon sequencing normalized to all bacterial 16S rRNA gene sequences. Colors distinguish MOB at the ASV level. **B)** *pmoA* transcript abundance derived from qPCR quantification (copies ml^{-1}) of *pmoA* multiplied with the relative abundance of *pmoA* mRNA aaASVs from pmoA amplicon sequencing. Colors correspond to aaASVs. ASVs and aaASVs which, based on multiple lines of evidence (see methods), are thought to originate from the same organism are encoded with the same color. **C)** MOB cell abundance as determined by CARD-FISH. **D)** Potential methane oxidation rates.

108

109

In the hypolimnion, other uncultivated type I MOB closely related to lacustrine Crenothrix prevailed (ASV_8, 35, 81, with 95.6-96.7% identity and aaASV2, 3, 8, with 96.1-97.4% identity to lacustrine Crenothrix; shown in shades of pink). In between the mixed layer and the methane-enriched hypolimnion the abundance of additional MOB sequences peaked, e.g. ASV_166 (Supplementary Fig. 5A) and aaASV12.

MOB dynamics at the onset of the overturn

By Oct 27 we observed an increase of MOB abundance and *pmoA* transcripts at the upper boundary of the methane-enriched hypolimnion (Fig. 2A, B). Although the mixed layer depth increased throughout October, it did not yet reach the methane-enriched hypolimnion (Fig. 2A, B). However, the deepening of the mixed layer brought oxygen-rich water closer to the hypolimnion, likely increasing the downward oxygen flux.

By Nov 9 the mixed layer had finally reached and eroded a small part of the methane-enriched hypolimnion (Fig. 2A, B). The MOB observed in the peak from Oct 27 had thus likely been entrained into the mixed layer. It is likely that both CABC2E06 (ASV_5/aaASV1 and 6, blue), as well as Crenothrix-related MOB (ASV_8/aaASV2, pink) were transported into the mixed layer. However, only the members of the CABC2E06 group (blue), which already prevailed in the mixed layer in October showed up as the dominant MOB in the expanding mixed layer (Fig. 2A, B, Supplementary Fig. 5). Thus, both transport of MOB to, and their growth in the mixed layer may have contributed to the increased MOB percentage and *pmoA* transcript numbers observed on Nov 9 (Fig. 2A, B). After this date, we no longer observed the MOB peak formation at the oxygen-methane interface typical for the stratified period, likely because the interface was now constantly moving downwards as the mixed layer deepened (Fig. 2A, B).

Dynamics of the MOB assemblage during the main phase of the overturn

From Nov 9 to Dec 12 the mixed layer deepened from 9 to 12 m, thereby incorporating large amounts of stored methane. It must be assumed that the MOB assemblage from the hypolimnion was continuously transported into the mixed layer. However, the Crenothrix-related MOB that dominated there (Fig. 2A, B) were only detected at very low abundances in the mixed layer. Instead, a MOB with 97.2% rRNA gene fragment sequence identity to *Methylosoma difficile* (ASV_12/aaASV5, Supplementary Fig. 4A) was rapidly increasing in abundance, peaking at a median percentage of 16% of all bacterial sequences in the mixed layer on Dec 12 (Fig. 2A, B, orange). At this date, all MOB sequences together reached up to 28% of the bacterial sequences, with ASV_12 as the most important contributor to the increase in MOB abundance. This taxon was already present in October, but at very low proportion with a maximum relative abundance of 0.2% of bacterial rRNA gene sequences.

In January, an inverse stratification formed and only close to the bottom of the lake (16 m max. depth) a small part of the water column retained stored methane. MOB proportion and mRNA copy numbers of ASV_12/aaASV5 decreased and the MOB assemblage shifted again, with ASV_15/aaASV4 (green, Fig. 2A, B) now dominating.

Dynamics of potential methane oxidation capacity and MOB cell numbers

In October, type I MOB cell numbers as determined by CARD-FISH peaked at the upper boundary of the methane-enriched hypolimnion, corroborating the patterns observed with MOB ASVs and *pmoA* mRNA transcripts. Further, potential methane oxidation rates showed a strikingly similar pattern, suggesting that the MOB assemblages were active. Even within the oxygen-depleted hypolimnion, potential methane oxidation rates never fell below 0.3 µM d^{-1} (Fig. 2C). Throughout the lake overturn, MOB cell numbers and potential methane oxidation rates increased substantially within the mixed layer (Fig. 2C, D). By Dec 12, the potential methane oxidation rates in the entire mixed layer exceeded the maximum rates during stable stratification, when maximum rates are usually confined to a narrow

156 layer at the oxygen-methane interface. The water volume capable of these high rates had thus
157 expanded significantly (Fig. 2D). In combination, this led to an overall increase of the potential
158 methane oxidation capacity in the mixed layer from 0.01 Mg C d^{-1} to 0.3 Mg C d^{-1} between October
159 and December (Fig. 2D) corresponding to a doubling of the rate every 12.7 days. At the same time,
160 MOB cell numbers in the mixed layer increased with a net doubling time of approximately 9 days.
161 After lake overturn was complete, i.e. between Dec 12 and Jan 23, potential methane oxidation rates
162 and MOB cell numbers generally decreased at the water depths formerly occupied by the mixed layer.
163 The methane oxidation rates and MOB abundance now increased with depth and peaked in the
164 remaining methane-enriched bottom layer near the sediment (Fig. 2C, D). All measured MOB
165 parameters were significantly correlated (Supplementary Tab. 1).

166 ## Winners and losers: thriving mixed layer MOB and fate of hypolimnetic MOB

167 The winners of the lake overturn were taxa of the mixed layer MOB assemblage (Fig. 3A), which
168 contributed substantially to the increase of potential methane oxidation rates (Fig. 3B). The profound
169 shift in the composition of the MOB assemblage suggested that the changing physical and chemical
170 conditions in the lake influenced the succession (Fig. 3 and Supplementary Fig. 3).

171

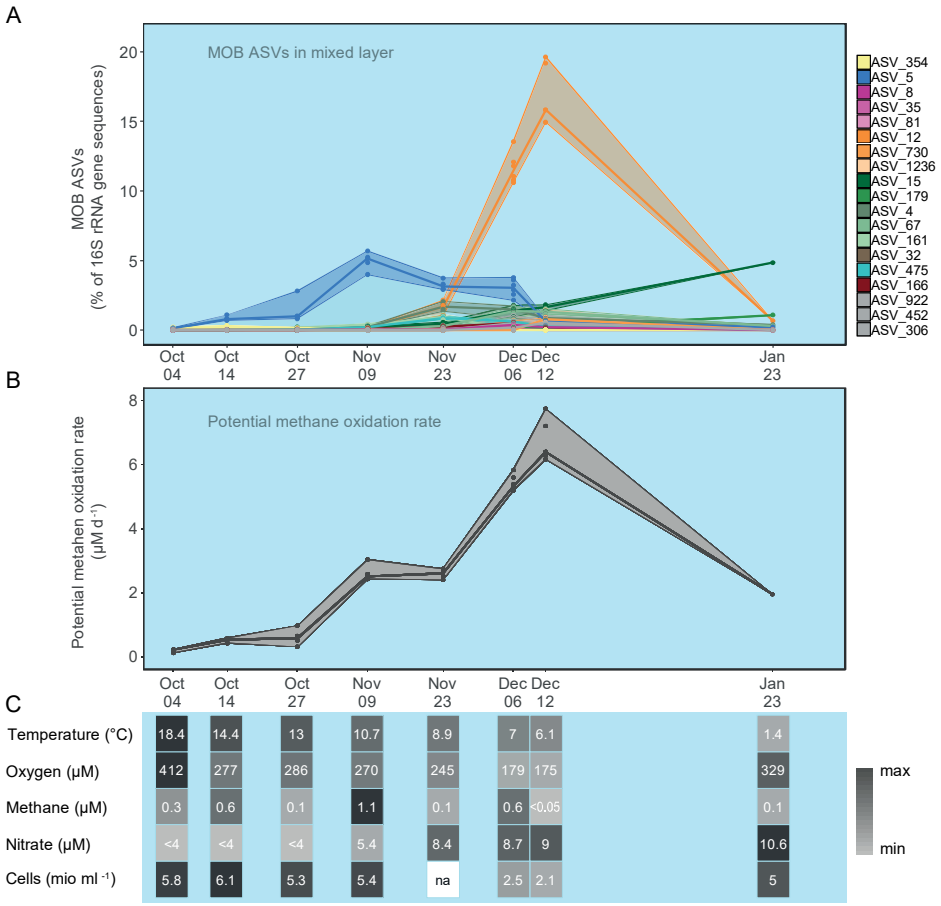

Figure 3 Mixed layer dynamics during lake overturn. **A)** MOB assemblage dynamics at the ASV level within the expanding mixed layer during lake overturn. Maximum, minimum and median relative abundance of each MOB ASV within the mixed layer are visualized with lines. Colors correspond to MOB ASVs. **B)** Dynamics of potential methane oxidation rates during lake overturn. Lines depict maximum, minimum and median within the mixed layer. **C)** Table illustrating the corresponding change in physical, chemical and biological environmental parameters in the mixed layer over time. The median of the mixed layer samples is shown for each parameter and sampling date. Shades of gray are scaled between minimum (light grey) and maximum (black) values. Values below the limit of quantification are marked with "<" and missing data with "na". Raw data for B and C are provided in Supplementary Table 2.

The dominance of CABC2E06 (ASV_5) in the oxygen-rich mixed layer until November supports previous observations of this taxon occurring under, and being correlated with, elevated oxygen concentrations during stable stratification in four Swiss lakes[16]. Our observations in this study further support the view that this MOB taxon thrives under high oxygen concentration and continuous but low-concentration methane supply. Despite its occurrence in several lakes and its sometimes high abundance and pivotal role during overturn, lack of a cultured representatives or genomes currently precludes further insights into the ecology of this taxon.

The early dominance of CABC2E06 (ASV_5) was followed by a pronounced increase of the *Methylosoma*-related ASV_12 until Dec 12, which led to dominance of this taxon during the lake overturn (orange, Fig. 3A). The growth phase of ASV_12 was accompanied by a drop in water temperature to below 10 °C, and increasing nutrient levels in the mixed layer (nitrate, Fig. 3C). The only cultured representative of *Methylosoma, M. difficile* is microaerophilic[17], which is in line with the observation that ASV_12 dominated during the period with the lowest measured oxygen concentration in the mixed layer (175 µM). This taxon was not observed in three other Swiss lakes in a previous study[16], and was only detected at very low abundance in the October samples of Rotsee in this campaign. This MOB taxon thus appears to be seasonally restricted or conditionally rare, but nevertheless was the most spectacular profiteer of the lake overturn and highly relevant to methane mitigation during our study period.

ASV_15, related to *Methylobacter tundripaludum* (98.6% identity) steadily increased during the later phase of the overturn and dominated the MOB assemblage on Jan 23. This finding could perhaps be explained by an adaptation of ASV_15 to low temperatures: lake water cooled to below 4°C in this period and oxygen levels replenished, while elevated nutrient levels persisted (Fig. 3C). Previous observations of psychrophily within the *Methylobacter* genus[18] provide some support for this hypothesis.

The losers of the lake overturn, Crenothrix-related ASVs/aaASVs (ASV_8, 35, 81 pink), remained restricted to the eroding hypolimnion, until only a tiny fraction was left on Jan 23 (Fig. 2A, B, Supplementary Fig. 5). The Crenothrix were never able to establish in the mixed layer, although these taxa were presumably inoculated continuously. This suggests that their ecological specialization may be responsible, as proposed earlier[16]. They resided in water layers with high methane concentrations and are thought to rely on oxygen released from phytoplankton[19] or from temporally and spatially limited nano- to micromolar oxygen intrusions[20]. On the other hand, the *Methylobacter tundripaludum*-like ASV_4 (99.3% identity) which was present at low abundance in the hypolimnion

205 gained momentum temporarily in the mixed layer in Nov and Dec (Fig. 3A), suggesting a comparatively

206 more flexible ecology for this organism.

Discussion

In this study, we provide the first comprehensive analysis of the response of a MOB assemblage to autumn lake overturn. We asked if the MOB assemblage grows fast enough to oxidize the stored methane before outgassing. Our results show unambiguously that the MOB assemblage in the observed lake was indeed reacting fast enough to minimize outgassing of the GHG methane during a gradual lake overturn. MOB growth led to a substantial increase in MOB abundance until MOB made up 28% of the bacterial 16S rRNA gene sequences in the mixed layer (Fig. 2). This established a high methane oxidation capacity in the expanding mixed layer. We further asked whether the standing MOB assemblage is activated, or a new assemblage successively takes over. We found that a temporal succession of MOB taxa underpins the increasing MOB abundance and methane oxidation capacity (Fig. 3A, B). Growth of a new MOB assemblage and its methane oxidation capacity limited the emitted methane to a small percentage of the stored methane during lake overturn (Zimmermann et al. 2019).

Beyond these main findings our work provides a number of insights into the ecology of freshwater MOB. There is some evidence that the successional patterns of MOB, similar to vertical niche preferences discussed previously[16] are related to specific adaptations of the successful taxa. During the phase with the highest methane oxidation capacity in the lake, the initial MOB assemblage of both, mixed layer and hypolimnion, had been almost entirely replaced by a new MOB assemblage (Fig. 2). Different MOB reached a high degree of dominance at different stages of the lake overturn, indicating that the changing environmental conditions favored temporal niche partitioning of MOB taxa (Fig. 3). It is notable, however, that despite the well-mixed situation and the often-observed dominance of a single taxon, a diverse MOB assemblage was nevertheless present throughout the overturn period. Answering the question whether the same or similar MOB are dominating the fall overturn every year will require a longer-term monitoring effort. Presence of MOB taxa with specific adaptation that allow them to take advantage of the rapidly changing conditions in the overturning lake is likely essential to establishing the methane oxidation capacity that ultimately limits methane outgassing.

Although methane becomes available in the mixed layer, dilution and rapid oxidation keep concentrations low as opposed to the situation in the hypolimnion (Fig. 3C). MOB in the mixed layer thus likely require a relatively high methane affinity for growth. We therefore speculate that the methane affinity of the mixed-layer MOB assemblage may be a critical factor for the amount of diffusive methane outgassing to the atmosphere during the overturn period. In addition to the inherent methane affinity of MOB taxa and assemblages, other traits like growth rates and ability to access nutrients likely affect the build-up of the methane-oxidation capacity in the lake and require further exploration.

The net doubling time of MOB in the expanding mixed layer of 9 days suggested slow growth, but MOB substantially increased their abundance and reached a total methane oxidation capacity in the mixed layer volume of approximately 0.3 Mg carbon per day (Dec 12). Our oxidation capacity estimate is conservative as only potential methane oxidation to CO_2 was measured and incorporation into biomass is not included. Even though the MOB growth rates seem low compared to observations in MOB isolates[21] they may be in line with the environmental conditions: temperatures in the mixed layer dropped from 18.4 (Oct 4) to 6.1°C (Dec 12), thus slowing process and growth rates are expected. Further, persistently low methane concentrations likely reduced effective growth rates. Because of the evident succession within the MOB assemblage, the doubling time given above represents a sum over all taxa and growth rates of e.g. taxa becoming dominant were certainly faster as other taxa stagnated or decreased in abundance at the same time. Finally, gross growth rates are likely higher as mortality rates remain unknown.

While some estimates of global methane emissions from lakes assume that all stored methane is emitted to the atmosphere[3,22], our data is in line with a number of field studies that suggest a considerable proportion of stored methane is oxidized. One study estimated that 46% of the stored methane is emitted during autumn lake overturn[8], but most estimates are higher, claiming oxidation of 75 – 94% of the stored methane[6,7,23]. Rotsee methane emission data from eddy-covariance flux

257 measurements and modelling[14] obtained in parallel with this study showed that in the present case
258 even about 98% of the stored methane was oxidized. Our data demonstrate that this outcome was
259 based on the robust response of MOB in the mixed layer where a succession of MOB maintained a
260 high methane oxidation capacity throughout the overturn. We must therefore caution against adding
261 methane storage to lake emission estimates. Certainly, lakes remain significant sources of
262 atmospheric methane: ebullition bypasses biological oxidation and rapid overturn events due to e.g.
263 fast lake cooling and strong winds will lead to increased outgassing[6,14]. Processes as observed in Rotsee
264 may occur in a considerable proportion of temperate lakes and might be important to global methane
265 flux estimates. Most lakes in temperate regions are holomictic and have a mean lake depth of < 25 m.
266 Worldwide, small (size classes 0.1-1 and 1-10 km^2), relatively shallow (average depth 5 and 5.4 m,
267 respectively) lakes represent 28% of the estimated global lake area[24] and methane storage is
268 frequently observed especially in small lakes[3]. The number of lakes with hypolimnetic methane
269 storage may increase in future due to lack of recovery of lakes from eutrophication[25] and continuing
270 eutrophication of other lakes[26], while global warming could strengthen summer stratification and, in
271 turn, methane accumulation. A comprehensive understanding on the fate of stored methane in
272 transitionally stratified lakes and information on the adaptability of MOB to different environmental
273 conditions and their methane oxidation kinetics are therefore critical.

274 In summary, we showed in this comprehensive study that successional changes in the MOB
275 assemblage of the mixed layer of an overturning lake secured high MOB abundance with an
276 extraordinarily high methane-oxidation capacity that significantly reduced the atmospheric emissions
277 of stored methane.

Methods

Environmental sampling and profiling during autumn overturn

A temperate holomictic lake, Rotsee (47.072 N and 8.319 E) in Central Switzerland was sampled on 8 dates from Oct 4, 2016 to Jan 23, 2017 (see Fig 1). This sampling period covered the end of stratification with maximal methane accumulation in the hypolimnion and the subsequent autumn overturn. A moored thermistor chain with 1 m resolution provided temperature measurements every three hours, documenting the mixing process and serving as a basis for scheduling the sampling dates. We defined the mixed layer depth as the part of the water column with a uniform temperature profile. At each sampling date, continuous profiles of temperature and oxygen (PSt1, Presens, Regensburg, Germany), were measured with the profiling *in-situ* analyzer (PIA) as described previously[27]. Sampling depths for further analyses were set based on the PIA profiles. The PIA was equipped with a syringe sampler for targeted depth sampling at 25 cm resolution, integrating about 5 cm water column, allowing for improved resolution compared to conventional Niskin bottle sampling which integrates over >50 cm.

Water samples for analysis of ammonium, nitrate and dissolved inorganic carbon (DIC) were filtered with a 0.2 µm pore size cellulose acetate filter (Sartorius, Göttingen, Germany) and stored at 4°C until analysis. Ammonium was measured by ion chromatography (Metrohm, Herisau, Switzerland) and nitrate with a flow-injection analyzer (SAN++, Skalar, Breda, The Netherlands). A total organic carbon analyzer (Shimadzu, Kyoto, Japan) was used for DIC quantification. Water samples for flow cytometry were fixed with formaldehyde and stained with SYBR Green I (Thermo Fisher Scientific, Waltham, MA, USA) at 37°C for 15 min. Particles were counted on an Accuri C6 flow cytometer (BD Biosciences, San Jose, CA, USA) and microbial cell counts determined as described previously[28].

Samples for methane measurements were injected into airtight 40 ml serum vials filled with N_2 gas and 4 g NaOH pellets (≥98% purity, Sigma-Aldrich, Darmstadt, Germany) for preservation. Gas

chromatography (6890N, Agilent Technologies, Santa Clara, CA, USA) was used to measure methane in the headspace. The GC was equipped with a Carboxen 1010 column (Supelco, Bellefonte, PA, USA) and a flame ionization detector. Control experiments showed that 4 g of solid NaOH released 32.6 nmol CH_4 on average which was accounted for when back-calculating methane concentrations in water based on Wiesenburg and Guinasso (1979)[29].

Nucleic acid purification

110 ml lake water were filtered on site through 0.2 µm cellulose acetate filters (Sartorius) and instantly frozen on dry ice. Samples were stored at -80 °C until extraction. Genomic DNA and total RNA were extracted from the same filter with the AllPrep DNA/RNA Mini Kit (Qiagen, Hilden, Germany) with a bead beating step on a FastPrep-24 (MP Biomedicals, Santa Ana, CA, USA) and 150-212 µm glass beads. Residual DNA in RNA extracts was digested using the TURBO DNA-free kit (Thermo Fisher Scientific). DNA removal was checked by gel electrophoresis after PCR (16S rRNA gene, 27f/1492r, 35 cycles) and if required, a second digestion was performed. If the second digestion was not sufficient to remove the DNA, the sample was excluded (one sample). cDNA was reverse transcribed from RNA with random hexamers using SuperScript IV First-Strand Synthesis System (Thermo Fisher Scientific). DNA and cDNA were used for Illumina MiSeq sequencing and qPCR.

16S rRNA and *pmoA* sequencing and analysis

Bacterial 16S rRNA gene and rRNA (S-D-Bact-0341-b-S-17, D-Bact-0785-a-A-21)[30] and functional marker *pmoA* gene and transcript (189f, mb661)[31] amplicon libraries were sequenced on the Illumina MiSeq platform (Illumina Inc., San Diego, CA, USA). Briefly, the first PCR was performed in triplicate with tailed forward and reverse primers using NEBNext Q5® Hot Start HiFi PCR Master Mix (New England BioLabs, Hitchin, UK) and 17 and 25 cycles for the bacterial and functional marker, respectively. Illumina barcodes and adapters were attached to pooled and purified products in a second PCR (8 cycles) with the Nextera XT Index Kit A and D (Illumina Inc.). Libraries were purified with

Agencourt AMPure XP kit (Beckman coulter, Indianapolis, IN, USA), quantified (Qubit, Thermo Fischer Scientific) and pooled. After quality check on a Tape Station 2200 (Agilent Genomics, USA) the two sequencing runs with 600-cycle MiSeq reagent kit v3 and 10% PhiX were performed at the Genetic Diversity Centre (ETH Zurich).

Amplicon sequence variants (ASVs) were inferred with the DADA2 pipeline[32] (v1.6.0) in R[33] (v3.4.1). Reads reaching a quality score of two were truncated and reads with ambiguous bases or an expected error rate exceeding three were removed. 16S rRNA reads were trimmed to 270 nt (forward) and 210 nt (reverse) and *pmoA* reverse reads were trimmed to 235 nt. The ASV table was produced following the DADA2 pipeline. Samples with less than 5000 reads were removed. Taxonomy of 16S rRNA ASVs was assigned using the SILVA reference database (v132)[34] and reads assigned to mitochondria or chloroplasts were removed with phyloseq[35] (1.24.2) in R (3.5.0). The 16S rRNA data set was screened for known methanotrophic groups[36] within the order *Methylococcales*, genera within class *Alphaproteobacteria* and phylum *Verrucomicrobia*, and *Candidatus* Methylomirabilis. ASVs reaching >0.2% relative abundance in at least 3 samples were retained for further analysis. To increase readability of Fig. 2 two samples (Oct 04) are not shown (7.25 m and 6.75 m), which does not change data interpretation. Amino acid sequences (aaASV) were derived from *pmoA* ASVs in MEGA7[37] and were retained for further analyses when exceeding 2% relative abundance in at least one sample. Neighbor-joining trees were constructed in MEGA7 with 10000 bootstrap replications using Jukes-Cantor evolutionary distance for 16S rRNA sequences or Poisson correction method for *pmoA* amino acid sequences. To facilitate interpretation we assigned the same colors for MOB ASVs (MOB-affiliated 16S rRNA amplicon sequence variants) and aaASVs (*pmoA* amino acid operational taxonomic units) if they (i) showed similar relative abundance and distribution patterns as observed in a canonical correspondence analysis (Supplementary Fig. 3), and (ii) if placement in the phylogenetic trees was compatible with this interpretation.

pmoA gene and transcript quantification

The amount of *pmoA* DNA and mRNA copies in lake water during overturn was quantified by qPCR using the 189f-mb661 primer pair[31] on a LightCycler 480 (Roche Diagnostics, Rotkreuz, Switzerland). 10µl reactions were performed with 0.2 µM primer, 2 µl of 1:10 diluted DNA or cDNA and the SYBR Green I Master mix (Roche). We used PCR conditions adapted from Henneberger et al. (2015)[38] with 10 min initial denaturation, 15 s denaturation during cycling and acquisition at 79°C. Standards were obtained by 10-fold serial dilution of *pmoA* containing plasmid, which were measured in quadruplicates. Sample assays were performed in triplicates and analysed with the LightCycler 480 software (v1.5.1.62) with the second derivative maximum method.

Potential methane oxidation rates

Water samples were filled into 60 ml serum vials in the field and laboratory incubations were started the same day. The applied procedure to determine potential methane oxidation was adapted from Oswald et al. 2015[19]. Each sample was purged with N_2 to remove residual methane, amended with non-limiting concentrations of oxygen (~50 µmol L^{-1}) and ^{13}C-CH_4 (~80 µmol L^{-1}), and subdivided into five Exetainers[39] (6ml) that were kept dark and close to the *in-situ* temperature of the mixed layer as determined at the date of sampling. Incubations were stopped after 0, 3, 13, 25 and 50 hours with 100 µl $ZnCl_2$ 50% w/v. The increase of ^{13}C-CO_2 was determined with GC-IRMS (IsoPrime, Micromass, Wilmslow, UK). Rates were derived from a linear regression of the ^{13}C-CO_2 production over time, taking into account the background DIC in the sample. Carrara marble (ETH Zurich, $\delta^{13}C$ of 2.1‰) served as a standard.

MOB quantification with CARD-FISH

To quantify MOB dynamics in terms of cell numbers we applied CARD-FISH. Samples were fixed with formaldehyde (2% final concentration) for 3-6 hours on ice prior to filtration onto 0.2 µm

polycarbonate nuclepore track-etched membrane filters (Whatman, Maidstone, UK). Dry filters were stored at -20°C until further processing. Filters were embedded in 0.2% low gelling point agarose (Metaphor, Lonza), cells were permeabilized with lysozyme (10 mg ml^{-1}) for 70 min at 37°C and peroxidases inactivated in 10 mM HCl for 10 min. The probes Mg84, Mg669 and Mg705[40] were mixed to target type I MOB. As control probes EUB338I-III (universal bacterial probe, positive control) and NON338 (negative control)[41,42] were separately applied to each sample. Filters were incubated at 46°C for 2.5 h with 150 µl of the respective hybridization buffer (20% formamide Mg-mix and 35% for EUB and NON) containing 1 µl of probe (50 ng $µl^{-1}$). After washing, filters were placed into the amplification buffer containing Oregon Green 488 at 37°C for 30 min in the dark. DAPI was used for counterstaining and the filters were mounted on glass slides in a mix of Citifluor and Vectashield (4:1).

Epifluorescence images were taken with an inverted microscope (DMI6000 B, Leica, Wetzlar, Germany) and a 100x/1.3 objective (PL-FL, Leica). To obtain clear images, multifocal images were recorded and merged with LASX software (Leica). DAPI and the corresponding CARD-FISH images of 22 randomly selected fields per filter were used for semi-automated cell counting with the daime (v 2.0) software[43]. In daime, image histograms were adjusted manually; objects were detected with the edge detection algorithm and split with a watershed segmentation-based algorithm. Object detection was improved manually if necessary. Median of cell numbers multiplied by the mixed layer volume were used to calculate growth rates (r) using the natural logarithm plotted against time (Oct – Dec 12). Doubling times were derived as dt = ln(2)/r (ref. 44).

Statistics

Canonical correspondence analysis (CCA) was performed with phyloseq[35] in R on the MOB ASV relative abundance among bacterial 16S rRNA gene sequences and the aaASV percentage of *pmoA* mRNA sequences. We used a Chi-square dissimilarity matrix and scaled physicochemical parameters (O_2 and CH_4 concentrations and temperature) as constraints. Constrained axes were tested for significance with anova.cca of vegan v2.5.2.

Spearman rank correlation between MOB parameters and potential methane oxidation rate were calculated in R and p values were adjusted for multiple comparisons using the Benjamini & Hochberg (BH) method.

The methane oxidation capacity was calculated based on the median potential methane oxidation rate in the mixed layer multiplied by the volume of the mixed layer.

Data availability

The sequencing files have been submitted to the European nucleotide archive under the project number PRJEB32413. All other data is available from the Eawag Research Data Institutional Collection (https://data.eawag.ch/dataset/growth-succession-of-methanotrophs-limit-methane-release-lake-overturn).

Acknowledgements

We thank Carsten Schubert and Serge Robert for access to the GC-IRMS and support with methane oxidation rate measurements and Carsten Schubert for his support, review of the manuscript, and helpful discussions. We thank Karin Beck, Patrick Kathriner, Miro Meyer and Michael Plüss for assistance in the field and laboratory. Sequencing data generation and analysis was done in collaboration with the Genetic Diversity Centre (GDC), ETH Zurich. The research was funded by Swiss National Science Foundation (grant CR23I3_156759).

Author contributions:

MM was responsible for carrying out the research, performed laboratory and data analysis and wrote the original manuscript. MZ and JD contributed methane oxidation rate measurements and JD contributed CARD-FISH analyses. MM, MZ, AB performed fieldwork. HB, BW, MZ contributed to

writing and reviewing and editing the manuscript. HB, BW, AB conceptualized and supervised the research, acquired funding and provided the research infrastructure.

Competing interests

The authors declare no competing interests.

References

1. DelSontro, T., Beaulieu, J. J. & Downing, J. A. Greenhouse gas emissions from lakes and impoundments: Upscaling in the face of global change. *Limnol. Oceanogr. Lett.* **3**, 64–75 (2018).

2. Bastviken, D., Ejlertsson, J. & Tranvik, L. Measurement of methane oxidation in lakes: A comparison of methods. *Environ. Sci. Technol.* **36**, 3354–3361 (2002).

3. Bastviken, D., Cole, J., Pace, M. & Tranvik, L. Methane emissions from lakes: Dependence of lake characteristics, two regional assessments, and a global estimate. *Global Biogeochem. Cycles* **18**, 1–12 (2004).

4. Myhre, G. *et al.* Anthropogenic and natural radiative forcing. in *Climate Change 2013: The Physical Science Basis. Contribution of Working Group I to the Fifth Assessment Report of the Intergovernmental Panel on Climate Change* (ed. Stocker, T.F., D. Qin, G.-K. Plattner, M. Tignor, S.K. Allen, J. Boschung, A. Nauels, Y. Xia, V. Bex, P. M. M.) 659–740 (Cambridge University Press, 2013).

5. Taipale, S., Kankaala, P., Hahn, M., Jones, R. & Tiirola, M. Methane-oxidizing and photoautotrophic bacteria are major producers in a humic lake with a large anoxic hypolimnion. *Aquat. Microb. Ecol.* **64**, 81–95 (2011).

6. Kankaala, P., Taipale, S., Nykänen, H. & Jones, R. I. Oxidation, efflux, and isotopic

fractionation of methane during autumnal turnover in a polyhumic, boreal lake. *J. Geophys. Res. Biogeosciences* **112**, 1–7 (2007).

7. Schubert, C. J., Diem, T. & Eugster, W. Methane emissions from a small wind shielded lake determined by eddy covariance, flux chambers, anchored funnels, and boundary model calculations: A comparison. *Environ. Sci. Technol.* **46**, 4515–4522 (2012).

8. Encinas Fernández, J., Peeters, F. & Hofmann, H. Importance of the autumn overturn and anoxic conditions in the hypolimnion for the annual methane emissions from a temperate lake. *Environ. Sci. Technol.* **48**, 7297–7304 (2014).

9. Oswald, K. *et al.* Crenothrix are major methane consumers in stratified lakes. *ISME J.* **11**, 2124–2140 (2017).

10. Biderre-Petit, C. *et al.* Identification of microbial communities involved in the methane cycle of a freshwater meromictic lake. *FEMS Microbiol. Ecol.* **77**, 533–545 (2011).

11. Blees, J. *et al.* Micro-aerobic bacterial methane oxidation in the chemocline and anoxic water column of deep south-Alpine Lake Lugano (Switzerland). *Limnol. Oceanogr.* **59**, 311–324 (2014).

12. Kojima, H., Iwata, T. & Fukui, M. DNA-based analysis of planktonic methanotrophs in a stratified lake. *Freshw. Biol.* **54**, 1501–1509 (2009).

13. Salcher, M. M. Same same but different: ecological niche partitioning of planktonic freshwater prokaryotes. *J. Limnol.* **73**, 74–87 (2014).

14. Zimmermann, M. *et al.* Lake overturn as a key driver for methane oxidation. *bioRxiv* (2019). doi:https://doi.org/10.1101/689182

15. Schubert, C. J. *et al.* Oxidation and emission of methane in a monomictic lake (Rotsee,

463 Switzerland). *Aquat. Sci.* **72**, 455–466 (2010).

464 16. Mayr, M. J., Zimmermann, M., Guggenheim, C., Brand, A. & Bürgmann, H. Niche partitioning
465 of methane-oxidizing bacteria along the oxygen-methane counter gradient of stratified lakes.
466 *ISME J (in press).*

467 17. Rahalkar, M. C., Bussmann, I. & Schink, B. Methylosoma difficile gen. nov., sp. nov., a novel
468 methanotroph enriched by gradient cultivation from littoral sediment of Lake Constance. *Int.*
469 *J. Syst. Evol. Microbiol.* **57**, 1073–1080 (2007).

470 18. Trotsenko, Y. A. & Khmelenina, V. N. Aerobic methanotrophic bacteria of cold ecosystems.
471 *FEMS Microbiol. Ecol.* **53**, 15–26 (2005).

472 19. Oswald, K. *et al.* Light-dependent aerobic methane oxidation reduces methane emissions
473 from seasonally stratified lakes. *PLoS One* **10**, 1–22 (2015).

474 20. Kirf, M. K. *et al.* Redox gradients at the low oxygen boundary of lakes. *Aquat. Sci.* **77**, 81–93
475 (2015).

476 21. Wise, M. G., McArthur, J. V & Shimkets, L. J. Methylosarcina fibrata gen. nov., sp. nov. and
477 Methylosarcina quisquiliarum sp.nov., novel type 1 methanotrophs. *Int. J. Syst. Evol.*
478 *Microbiol.* **51**, 611–621 (2001).

479 22. Bastviken, D., Cole, J. J., Pace, M. L. & Van de-Bogert, M. C. Fates of methane from different
480 lake habitats: Connecting whole-lake budgets and CH4 emissions. *J. Geophys. Res.*
481 *Biogeosciences* **113**, 1–13 (2008).

482 23. Utsumi, M. *et al.* Dynamics of dissolved methane and methane oxidation in dimitic Lak Nojiri
483 during winter. *Limnol. Oceanogr.* **43**, 10–17 (1998).

484 24. Messager, M. L., Lehner, B., Grill, G., Nedeva, I. & Schmitt, O. Estimating the volume and age

485 of water stored in global lakes using a geo-statistical approach. *Nat. Commun.* **7**, 1–11 (2016).

486 25. Jenny, J.-P. *et al.* Urban point sources of nutrients were the leading cause for the historical
487 spread of hypoxia across European lakes. *Proc. Natl. Acad. Sci.* **113**, 12655–12660 (2016).

488 26. Beaulieu, J. J., DelSontro, T. & Downing, J. A. Eutrophication will increase methane emissions
489 from lakes and impoundments during the 21st century. *Nat. Commun.* **10**, 1375 (2019).

490 27. Kirf, M. K., Dinkel, C., Schubert, C. J. & Wehrli, B. Submicromolar oxygen profiles at the oxic-
491 anoxic boundary of temperate lakes. *Aquat. Geochemistry* **20**, 39–57 (2014).

492 28. Proctor, C. R. *et al.* Phylogenetic clustering of small low nucleic acid-content bacteria across
493 diverse freshwater ecosystems. *ISME J.* **12**, 1344–1359 (2018).

494 29. Wiesenburg, D. A. & Guinasso, N. L. Equilibrium solubilities of methane, carbon monoxide,
495 and hydrogen in water and sea water. *J. Chem. Eng. Data* **24**, 356–360 (1979).

496 30. Klindworth, A. *et al.* Evaluation of general 16S ribosomal RNA gene PCR primers for classical
497 and next-generation sequencing-based diversity studies. *Nucleic Acids Res.* **41**, 1–11 (2013).

498 31. Costello, A. M. & Lidstrom, M. E. Molecular characterization of functional and phylogenetic
499 genes from natural populations of methanotrophs in lake sediments. *Appl. Environ. Microbiol.*
500 **65**, 5066–74 (1999).

501 32. Callahan, B. J. *et al.* DADA2 : High resolution sample inference from amplicon data. *Nat.*
502 *Methods* **13**, 581–583 (2016).

503 33. R Core Team. A language and environment for statistical computing. (2017).

504 34. Quast, C. *et al.* The SILVA ribosomal RNA gene database project: Improved data processing
505 and web-based tools. *Nucleic Acids Res.* **41**, 590–596 (2013).

506 35. McMurdie, P. J. & Holmes, S. Phyloseq: An R Package for Reproducible Interactive Analysis
507 and Graphics of Microbiome Census Data. *PLoS One* **8**, 1–11 (2013).

508 36. Knief, C. Diversity and habitat preferences of cultivated and uncultivated aerobic
509 methanotrophic bacteria evaluated based on pmoA as molecular marker. *Front. Microbiol.* **6**,
510 1–38 (2015).

511 37. Kumar, S., Stecher, G. & Tamura, K. MEGA7: Molecular evolutionary genetics analysis version
512 7.0 for bigger datasets. *Mol. Biol. Evol.* **33**, 1870–1874 (2016).

513 38. Henneberger, R. *et al.* Field-scale tracking of active methane-oxidizing communities in a
514 landfill cover soil reveals spatial and seasonal variability. *Environ. Microbiol.* **17**, 1721–1737
515 (2015).

516 39. Holtappels, M., Lavik, G., Jensen, M. M. & Kuypers, M. M. M. 15N-labeling experiments to
517 dissect the contributions of heterotrophic denitrification and anammox to nitrogen removal
518 in the OMZ waters of the ocean. *Methods Enzymol.* **486**, 224–246 (2011).

519 40. Eller, G., Stubner, S. & Frenzel, P. Group-specific 16S rRNA targeted probes for the detection
520 of type I and type II methanotrophs by fluorescence in situ hybridisation. *FEMS Microbiol.*
521 *Lett.* **198**, 91–97 (2001).

522 41. Daims, H., Brühl, A., Amann, R., Schleifer, K. H. & Wagner, M. The domain-specific probe
523 EUB338 is insufficient for the detection of all bacteria: Development and evaluation of a more
524 comprehensive probe set. *Syst. Appl. Microbiol.* **22**, 434–444 (1999).

525 42. Wallner, G., Amann, R. & Beisker, W. Optimizing fluorescent in sit hybridization with rRNA-
526 targeted oligonucleotide probes for flow cytometric identification of microorganisms.
527 *Cytometry* **14**, 136–143 (1993).

528 43. Daims, H., Lücker, S. & Wagner, M. Daime, a Novel Image Analysis Program for Microbial
529 Ecology and Biofilm Research. *Environ. Microbiol.* **8**, 200–213 (2006).

530 44. Graham, L. E., Graham, J. M. & Wilcox, L. W. *Algae*. (Pearson Benjamin Cummings, 2009).

531